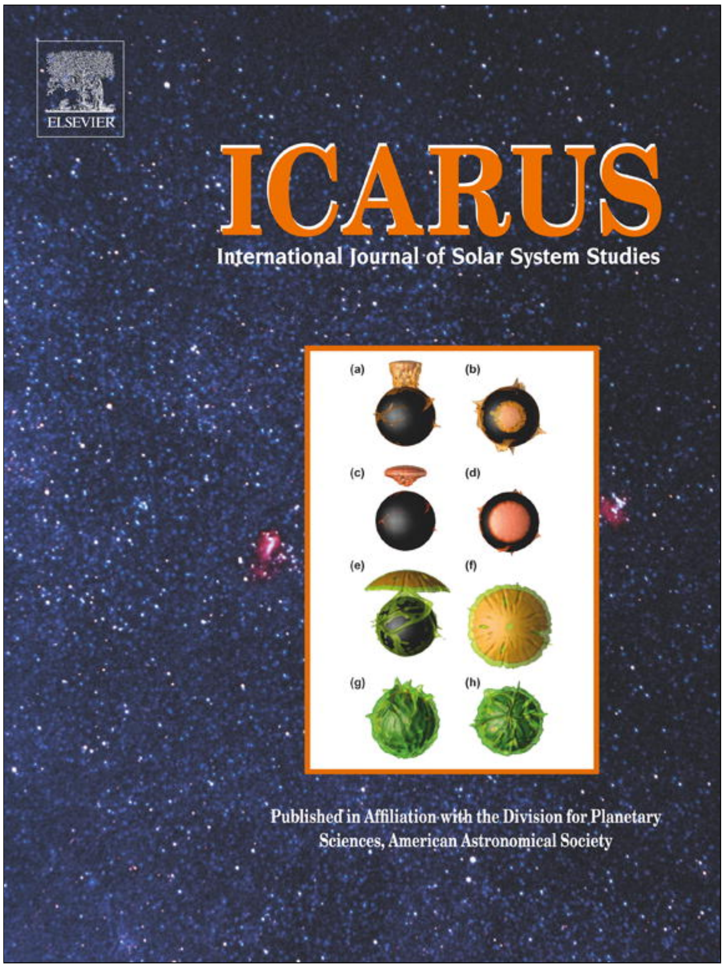
ELSEVIER
ICARUS
International Journal of Solar System Studies
(a)
(b)
(c)
(d)
(e)
(f)
(g)
(h)
Published in Affiliation with the Division for Planetary Sciences, American Astronomical Society

Icarus 223 (2013) 330–343

Contents lists available at SciVerse ScienceDirect

Icarus

journal homepage: www.elsevier.com/locate/icarus

Impact of a new wavelength-dependent representation of methane photolysis branching ratios on the modeling of Titan's atmospheric photochemistry

B. Gans [a], Z. Peng [b], N. Carrasco [c], D. Gauyacq [a], S. Lebonnois [d], P. Pernot [b,*]

[a] Institut des Sciences Moléculaires d'Orsay, UMR 8214, CNRS, Univ Paris-Sud, F-91405 Orsay, France
[b] Laboratoire de Chimie Physique, UMR 8000, CNRS, Univ Paris-Sud, F-91405 Orsay, France
[c] Université de Versailles Saint-Quentin, CNRS/INSU, LATMOS, UMR 8190, F-78280 Guyancourt, France
[d] Laboratoire de Météorologie Dynamique, Université Paris 6, F-75006 Paris, France

ARTICLE INFO

Article history:
Received 29 June 2012
Revised 9 November 2012
Accepted 13 November 2012
Available online 3 December 2012

Keywords:
Titan
Atmospheres, Chemistry
Atmospheres, Composition
Photochemistry

ABSTRACT

A new wavelength-dependent model for CH_4 photolysis branching ratios is proposed, based on the values measured recently by Gans et al. (Gans, B. et al. [2011]. Phys. Chem. Chem. Phys. 13, 8140–8152). We quantify the impact of this representation on the predictions of a photochemical model of Titan's atmosphere, on their precision, and compare to earlier representations. Although the observed effects on the mole fraction of the species are small (never larger than 50%), it is possible to draw some recommendations for further studies: (i) the Ly-α branching ratios of Wang et al. (Wang, J.H. et al. [2000]. J. Chem. Phys. 113, 4146–4152) used in recent models overestimate the CH_2:CH_3 ratio, a factor to which a lot of species are sensitive; (ii) the description of out-of-Ly-α branching ratios by the "100% CH_3" scenario has to be avoided, as it can bias significantly the mole fractions of some important species (C_3H_8); and (iii) complementary experimental data in the 130–140 nm range would be useful to constrain the models in the Ly-α deprived 500–700 km altitude range.

1. Introduction

Titan, the largest satellite in the kronian system, has a massive atmosphere of 1.5 bar at the surface, extending up to about 1500 km of altitude. Methane is its second most abundant constituent after nitrogen and participates for about 2–10% of the total composition depending on the altitude (Hébrard et al., 2007).

With such a massive and extended atmosphere, the radiative budget of Titan's atmosphere is complex, controlled by a progressive and selective absorption of the solar spectrum from the top of the atmosphere down to the surface by nitrogen and methane, but also by minor compounds produced by atmospheric photochemistry. Actually the combined photochemistry coupling nitrogen and methane systems leads to the production of heavier volatile organic species, but also to nitrogen-rich solid organic aerosols with a strong prebiotic interest starting from the upper layers of Titan's atmosphere (Waite et al., 2007).

The photolysis of methane is one of the central primary processes initiating the unique radical and ion chemistry network of "Titan's organic factory" (Atreya, 2007). Its influence on Titan's atmospheric chemical species has been quantified in the global sensitivity study led in Hébrard et al. (2009). This work shows that methane photolysis is a key process at altitudes as low as 600 km, with an increasing weight in the upper atmosphere.

Methane photolysis in the upper layers of the atmosphere is mainly driven by the Ly-α wavelength (121.6 nm), for which experimental fragmentation probabilities are available. However, this predominance disappears below ~700 km, and the evolution of the methane fragmentation pattern with wavelength can affect the photochemistry occurring at various altitudes in Titan's atmosphere. The variation of the branching ratios among the products of methane photolysis at other wavelengths than Ly-α is mostly unexplored, and recent results by Gans et al. (2011) shed a new light on this topic.

To assess the influence of the values of these branching ratios in a photochemical model of Titan's atmosphere, a local sensitivity study was performed by Wilson and Atreya (2000) for hydrocarbon species. Varying methane photodissociation branching ratios sequentially at Ly-α and in the rest of the spectral range, they found a significant effect of the Ly-α branching ratios for heavier species (containing more than two carbon atoms). But, the effect of non-Ly-α branching ratios was found to be small, modifying at most C_2H_6 density by 65%. In this study however, Ly-α remains the main contribution to methane photolysis down to 600 km.

The aim of the present article is to quantify the impact of the new measurements of methane photolysis branching ratios by Gans et al. (2011) on the predictions of a photochemical model of Titan's atmosphere, and on their precision. In the next section,

* Corresponding author.
E-mail address: pascal.pernot@u-psud.fr (P. Pernot).

0019-1035/$ - see front matter © 2012 Elsevier Inc. All rights reserved.
http://dx.doi.org/10.1016/j.icarus.2012.11.024

we review the existing experimental data on the VUV fragmentation of methane, their implementation in recent photochemical models, and the expected contribution of non-Ly-α wavelengths to Titan's photochemistry. In Section 3, we develop a wavelength-dependent model for methane photolysis branching ratios, building on recent developments in the probabilistic representation of uncertain branching ratios (Plessis et al., 2010, 2011). This model is then implemented in a 1D photochemical model of Titan's atmosphere and used for a comparison of the predicted densities of minor chemicals with those produced by the dichotomous Ly-α/non-Ly-α representation. The results are presented and discussed in Section 4. We conclude by providing insights for the impact of the present wavelength-dependent model in other, non-Ly-α dominated, radiation fields (synchrotron, intergalactic, etc.). Motivated data needs for Titan's atmosphere modeling are also presented.

2. VUV photolysis of methane: data and models

We review in this section the existing data on the photodissociation of methane on the experimental side, notably recent data for a non-Ly-α wavelength. Next, we consider the status of the implementation of the photolysis branching ratios data in photochemical models of Titan's upper atmosphere.

2.1. Review of the experimental and theoretical data

Photodissociation of methane has long provided serious challenges both to theory and experiments. One of the first factors which make the quantitative description of methane photolysis challenging is that several energetically allowed fragmentation channels are open, following excitation at the VUV wavelengths. The seven spin-allowed and thermodynamically-open dissociation channels at the Ly-α wavelength (λ = 121.6 nm = 10.2 eV) are listed in Table 1.

On the experimental side, the challenge comes from the difficulty of quantitatively probing the fragments such as CH_2 and CH_3. If we consider only collision-free experimental studies on the photodissociation of methane, several earlier studies have been performed, particularly at Ly-α, all of them being mainly focused on the H atom fragment detection. Mordaunt et al. (1993) estimated the quantum yield for the H atom, Φ(H) = 1.0 ± 0.5. Soon after, Brownsword et al. (1997) reinvestigated the Ly-α photolysis of methane and found a much smaller value for the H quantum yield, Φ(H) = 0.47 ± 0.11. The H/D atom kinetic energy distribution after photodissociation of methane and its deuterated isotopomers, was revisited by Wang and Liu (1998) and Wang et al. (2000). A more recent work on the H atom detection by laser induced fluorescence led to a still different value for the H atom quantum yield (Φ(H) = 0.31 ± 0.05) (Park et al., 2008), which did not help to clarify the landscape of methane photolysis. Lately, Zhang et al. (2010) performed high resolution H atom Rydberg tagging time-of-flight spectra following the photolysis of methane at wavelengths between 128 and 130 nm. They interpreted their data by inferring very highly rotationally excited CH_3 fragments. Nevertheless, their fragment internal energy analysis in terms of pure rotational excitation is questionable and should deserve a more careful simulation of the internal energy distribution.

On the theoretical side, a complete quantitative description would imply to follow the seven aforementioned channels through adiabatic and non-adiabatic trajectories on the 9-dimensional potential energy surfaces (PES). Unfortunately, these calculations have not been performed yet. MRCI and EOM-CCSD approaches were used by Mebel et al. (1997) and gave the first evidence of local minima in the S_1 first excited surface of the 3s $^1T_2$ state of CH_4. This work was completed by *ab initio* calculations performed by Cook et al. (2001), who studied other regions of this S_1 surface but none of these studies could extract possible pathways, either adiabatic or non-adiabatic, leading to methane dissociation. Later, Van Harrevelt (2006) presented a study based on MR-SDCI calculations allowing to explore possible non-adiabatic pathways towards methane dissociation. He found that some of the minima previously calculated by Mebel et al. (1997) were in fact saddle points. He found the occurrence of conical intersection between the S_1 and the S_0 surfaces which would possibly lead to the formation of CH_3(X) and CH_2(a), in addition to the allowed dissociation into CH_2(X) on the S_1 PES. Furthermore, he calculated the absorption cross section by MCTDH for excitation energies between 9 and 11 eV (137.8–112.7 nm). Then, by deconvolving the calculated absorption cross section by a semi-classical method, he could extract the contributions of the three Jahn–Teller distorted components of the S_1 state reached by VUV absorption (Van Harrevelt, 2007) (Fig. 1). The only available complete calculation of the dissociation pathways, via Trajectory Surface Hopping classical trajectory calculations, has been proposed by Lodriguito et al. (2009), but with much less accurate potential energy surfaces. These authors could derive branching ratios for methane photolysis which, according to them, "unexpectedly" fitted the experimental

Table 1
New branching ratios for methane photolysis channels at 121.6 nm and 118.2 nm with 1σ standard uncertainties (Gans et al., 2011).

	Dissociation channel	Notation in models	Branching ratio at 121.6 nm	Branching ratio at 118.2 nm
(1)	$CH_3(X^2A_2'') + H$	CH_3	$\Phi(1) = 0.42 \pm 0.05$	$\Phi(1) = 0.26 \pm 0.04$
(2)	$CH_2(a^1A_1) + H_2$	$^1CH_2$	$\Phi(2) = 0.48 \pm 0.05$	$\Phi(2) + \Phi(3) = 0.17 \pm 0.05$
(3)	$CH_2(a^1A_1) + 2H$		$\Phi(3) \approx 0$	
(4)	$CH_2(b^1B_1) + H_2$	–	$\Phi(4) \approx 0$[a]	$\Phi(4) \approx 0$[a]
(5)	$CH_2(X^3B_1) + 2H$	$^3CH_2$	$\Phi(5) = 0.03 \pm 0.08$	$\Phi(5) = 0.48 \pm 0.06$
(6)	$CH(X^2\Pi) + H + H_2$	CH	$\Phi(6) = 0.071$[b]	$\Phi(6) = 0.097$[b]
(7)	$C(^1D) + 2H_2$	–	$\Phi(7) = 0 \pm 0.006$	$\Phi(7) = 0 \pm 0.006$

[a] From Lee and Chiang (1983).
[b] Interpolated from Rebbert and Ausloos (1972/73).

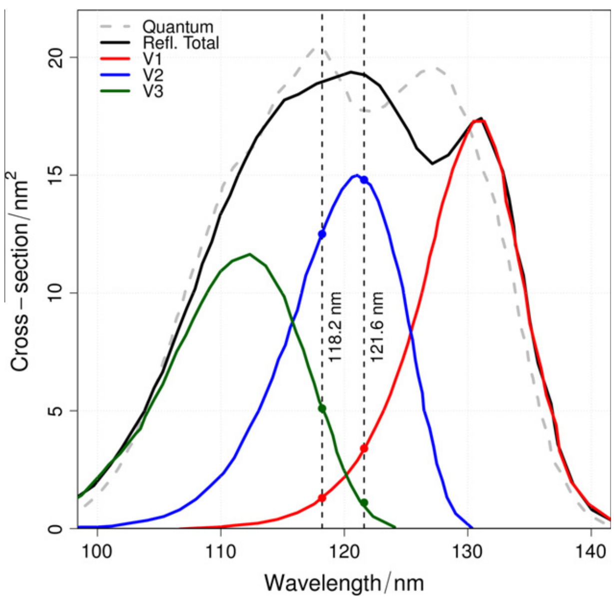

Fig. 1. Decomposition of the methane absorption cross-section into 3 bands according to Van Harrevelt (2007) (see text for details). This model could qualitatively explain the measured difference between the branching ratios at 118.2 and 121.6 nm (Section 2.2), and hints at a smooth variation of branching ratios with wavelength, as used in the proposed wavelength-dependent model (Section 3).

results of Wang et al. (2000) and Brownsword et al. (1997), given the lack of accuracy of their approach.

These recent papers indicate that, although a considerable experimental and theoretical effort has been carried out on methane photolysis over the last two decades, a large uncertainty still remains on the products quantum yields. One of the sources of uncertainty is related to the H atom product distribution and more particularly to its quantum yield. Another strategy has been proposed recently (Gans et al., 2010, 2011), based on the detection of carbon-bearing fragments CH_3 and CH_2 as detailed below.

2.2. Measurements by Gans et al. (2011) at 121.6 nm and 118.2 nm

Recently, new measurements of methane photolysis branching ratios have been performed at 121.6 nm and 118.2 nm by Gans et al. (2011). This study has been focused on the major channels leading to CH_3 and CH_2 radicals with careful uncertainty determination. The main results of this study are reported in Table 1. A key finding is that these branching ratios are strongly wavelength-dependent (Table 1, Fig. 2) which points to the need to revisit their implementation in photochemical models.

The large difference between the branching ratios at the two photolysis wavelengths 121.6 nm and 118.2 nm, shown in Fig. 2, is most probably due to the complex topology of the first excited singlet PES of methane, and can be rationalized by considering the absorption cross section calculations by Van Harrevelt (2007), shown in Fig. 1. Indeed, after photoexcitation of CH_4, the molecule may follow different routes towards dissociation on the three Jahn–Teller distorted surfaces arising from the $^1T_2$ degenerate excited state. The three electronic surfaces resulting from the lift of degeneracy upon distortion of the molecule, are optically reached via the three excitation probabilities represented by the V1, V2 and V3 components, obtained by deconvolving the theoretical absorption spectrum of Fig. 1 (Van Harrevelt, 2007). These energy surfaces lead to different dissociation products either by direct dissociation or by internal conversion towards the ground state S_0 surface, or by intersystem crossing towards a lower lying triplet state. In Fig. 1, the probability of populating the intermediate PES (V2 component) dominates at both wavelengths, nevertheless a drastic change occurs between the two photolysis wavelengths on what concerns V1 and V3 components, which might result into noticeably different dissociation dynamics and thus different branching ratios.

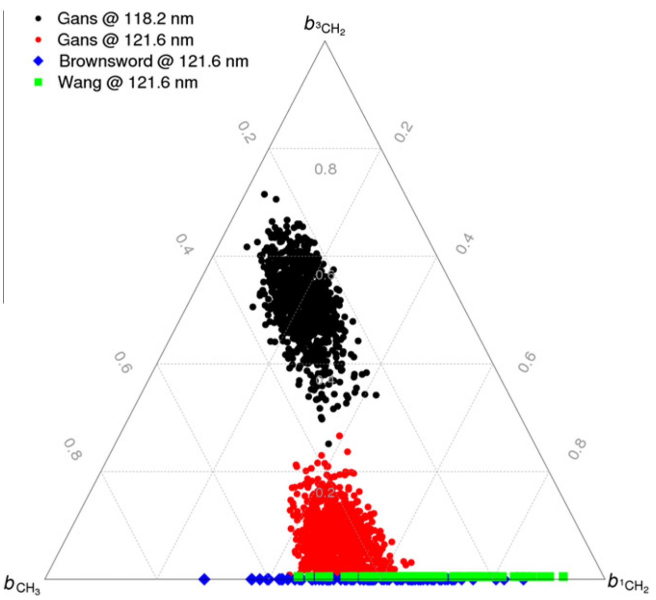

Fig. 2. Experimental branching ratios for CH_3, $^3CH_2$ and $^1CH_2$ at two wavelengths $\lambda = 118.2$ nm ("Gans @ 118.2 nm"; black bullets) and $\lambda = 121.6$ nm ("Gans @ 121.6 nm"; red bullets), from Gans et al. (2011). Other data are representative samples generate from Brownsword et al. (1997) ("Brownsword @ 121.6 nm"; blue diamonds) and Wang et al. (2000) ("Wang @ 121.6 nm"; green squares). (For interpretation of the references to color in this figure legend, the reader is referred to the web version of this article.)

Fig. 2 also reports the results of Brownsword et al. (1997) and Wang et al. (2000), which are the most currently used in planetary models (see Section 2.3), but which both rely on the very controversial value of the H atom quantum yield. Representative samples have been generated from the uncertainties estimated in these references. Note that the dissociative channel leading to the $CH_2(X)$ radical ($^3CH_2$) was completely neglected by these authors. Thus, the corresponding branching ratio is set to zero without dispersion.

2.3. Implementation of VUV methane photolysis in models

Until recently, the lack of knowledge about the branching ratios of methane photolysis at wavelengths other than Ly-α led modelers to treat separately Ly-α and the rest of the solar spectrum (non-Ly-α). In the following, this approach is referred to as "dichotomous", by opposition to wavelength-continuous models.

The representations of methane branching ratios used in a set of 1D models developed to describe Titan's photochemistry are gathered in Table 2. In the following, we adopt for the fragments of CH_4 the *de facto* standard notation in modeling literature, using the spin state of the CH_2 fragment, as given in Table 1.

Methane photolysis can lead to the production of $^1CH_2$ with two possible co-products: molecular hydrogen H_2 or atomic hydrogen H. As discussed in Wilson and Atreya (2009), the atmospheric impact of both hydrogen forms is very different. Molecular hydrogen, less reactive is mainly lost by thermal escape, whereas atomic hydrogen is efficiently involved in Titan's atmospheric chemistry. These two pathways are therefore considered separately in models. Nevertheless, Gans et al. (2011) showed that Wang et al. (2000) miscalculated the partition between both pathways, and that actually the "H+H" pathway is negligible in comparison to the "H_2" one. The branching ratios reported in Table 2 neglects this effect by summing the contributions of both pathways.

Successive experimental studies modified strongly the way methane photolysis is represented in Titan's photochemical models through time (Table 2). Models were first driven by the work of Mordaunt et al. (1993), predicting an almost equal distribution between CH_3 and CH fragments, without any CH_2 production (neither $^1CH_2$ nor $^3CH_2$). Independently, Romani (1996) fitted a new scheme from the data of Mordaunt et al. (1993) and constraints on H_2, H and CH quantum yields. The corresponding Ly-α branching ratios were in good agreement with the experimental data published slightly later by Brownsword et al. (1997). They were used by Wilson and Atreya (2004) and De La Haye et al. (2008). The measurements of Wang et al. (2000) changed again drastically the distribution among the methane fragments, showing that CH_3 had been overestimated at the detriment of CH_2, and have been used in most recent models.

Despite this updating of the branching ratios at Ly-α, the common scheme is to consider the production of a single fragment for wavelengths out of Ly-α, generally CH_3. An exception is Lebonnois et al. (2001), who considered the production of $^1CH_2$. With the data of Wang et al. (2000) placing CH_2 as the major fragment at Ly-α, this option could have become more popular, but other options have appeared.

Since 2009, a new interest is given to methane photolysis out of Ly-α, as can be seen in Table 2. The arbitrary rule "$b_{CH_3} = 1$ out of Ly-α" tends to disappear in favor of a uniform extension of Ly-α branching ratios to the whole VUV wavelength range (above 95 nm).

Table 2
Methane neutral photodissociation branching ratios, as implemented in various 1D-models of Titan's atmospheric chemistry. We consider only the wavelength range above methane ionization threshold at 95 nm.

Source	Ly-α				Titan model	Non-Ly-α
	b_{CH_3}	$b_{^1CH_2}$	$b_{^3CH_2}$	b_{CH}		
Mordaunt et al. (1993)	0.49	0.00	0.00	0.51	Lara et al. (1996)	$b_{CH_3} = 1$
					Lebonnois et al. (2001)	$b_{^1CH_2} = 1$
Romani (1996)	0.41	0.28	0.21	0.10	Wilson and Atreya (2004) and De La Haye et al. (2008)	$b_{CH_3} = 1$
Wang et al. (2000)	0.29	0.64	0.00	0.07	Hébrard et al. (2006) and Lavvas et al. (2008)	$b_{CH_3} = 1$
					Wilson and Atreya (2009)	N/A
					Krasnopolsky (2009) and Lavvas et al. (2011)	id. Ly-α
Gans et al. (2011)	0.42	0.48	0.03	0.07	This work	Wavelength-dependent

The new data by Gans et al. (2011), displaying a remarkable redistribution of branching ratios between 121.6 nm and 118.2 nm incited us to question these uniform extrapolations and to design a continuous wavelength-dependent representation of the branching ratios (see Section 3).

2.4. Contributions of Ly-α vs. non-Ly-α wavelengths to the photolysis rate of CH_4

At the outer limit of a pure CH_4 atmosphere undergoing solar irradiation, the Ly-α absorption would represent about 70% of the full absorption, with about 20–25% of photons absorbed at smaller wavelengths. If we account for a N_2:CH_4 = 0.97:0.03 mixing ratio, the photons below 100 nm are mostly absorbed by N_2, and the importance of Ly-α for the photolysis of CH_4 is notably increased, to about 90%. The cross-sections and solar flux used to compute these estimations are reported in Fig. 3.

To picture the situation at lower altitudes, a 1D radiative transfer model can be used to compute the wavelength and altitude-dependent photolysis rate of CH_4, $J_\lambda(z)$. Details of the model can be found in Peng et al. (2012). Fig. 4 shows the weighted photolysis rates $W_\lambda(z) = J_\lambda(z)/\bar{J}(z)$, providing the relative contributions of different wavelength groups to methane destruction. Note that to enhance the color contrast for low values of $W_\lambda(z)$, we plotted a monotonous transform of this quantity: $-\ln(1/W_\lambda(z) - 1)$. The top panel displays $W_\lambda(z)$ at the top of the atmosphere. In this region, besides the main peak around Ly-α, a weak contribution is observed at about 95 nm, within N_2 absorption range. The other peaks should not contribute significantly. If one considers the lower panel of Fig. 4, one can see the evolution of $W_\lambda(z)$ as a function of altitude. The Ly-α peak contributes predominantly from the top down to 650 km, where the main absorption is shifted to 135–145 nm, notably because of the presence of peaks in the solar flux at 130 nm, 133 nm and 140 nm, and of the fast increase of the solar flux in this range (Fig. 3).

Non-Ly-α wavelengths are thus expected to contribute significantly to the fragmentation of methane below 700 km.

3. Methods and models

The previous section showed that a wavelength-dependent representation of branching ratios is needed to account for the recent

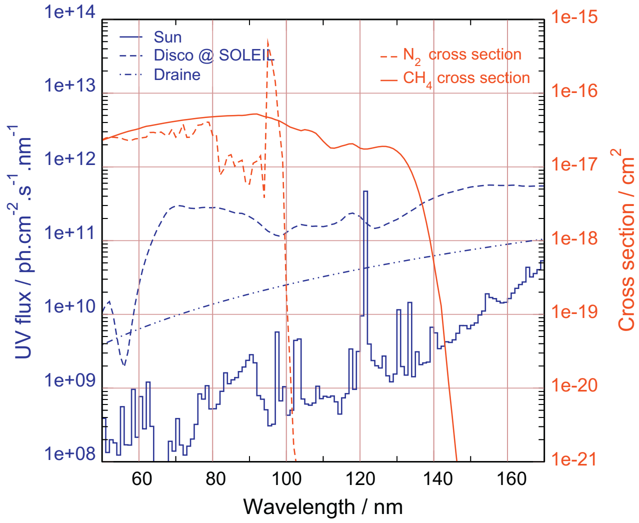

Fig. 3. Representative VUV radiation fields: (blue/full) solar; (blue/dash) synchrotron DISCO line at SOLEIL (Giuliani et al., 2009); and (blue/dot-dash) Draine's average galactic (van Dishoeck and Black, 1982)) and photoabsorption cross-section for N_2 (red/dash) and CH_4 (red/full). (For interpretation of the references to color in this figure legend, the reader is referred to the web version of this article.)

data and the expected interest of non-Ly-α wavelengths to the chemistry of Titan's atmosphere. This section introduces a new, wavelength-dependent, model for branching ratios of methane photolysis and presents the Monte Carlo procedure used to implement this model in photochemical simulations. The 1D photochemical code used in the application is also briefly introduced.

3.1. Probabilistic tree representation of sets of uncertain branching ratios

When dealing with uncertain parameters, special attention has to be paid to non-independent parameters, which is the case of branching ratios. For a reaction with n product channels, the branching ratios b_i have two constraints ($b_i \geqslant 0$ and $\sum_{i=1}^{n} b_i = 1$), which define them as probabilities. It has been shown that enforcing the sum-to-one is essential to ensure that, when estimating uncertainties of the outputs of a chemical model, uncertainty on branching ratios of a given reaction does not propagate to unrelated products (Carrasco and Pernot, 2007).

For some processes, as electron impact with ions (Plessis et al., 2010) or photodissociation (Gans et al., 2011), the set of branching ratios is heterogeneous, in the sense that subsets of data are derived from different experimental setups. In such cases, a practical way to impose the sum-to-one over the whole set while preserving the statistical independence between subsets is to use *probabilistic trees* (Plessis et al., 2010). A probabilistic tree is a hierarchy of branching ratios sets, such that, at each node, contributions sum to 1 (represented in the schemes below by a brace '{').

From the available information on CH_4 photolysis reported in Table 1, i.e. separate measurements for $\Phi_\lambda(6)$ and the other non-zero branching ratios, we can build a probabilistic tree accounting for the four observed pathways

$$CH_4 + h\nu(\lambda) \rightarrow \begin{cases} \overset{B_1(\lambda)}{\rightarrow} \begin{cases} \overset{B_{11}(\lambda)}{\rightarrow} CH_3 + H \\ \overset{B_{12}(\lambda)}{\rightarrow} {}^1CH_2 + H_2 \\ \overset{B_{13}(\lambda)}{\rightarrow} {}^3CH_2 + 2H \end{cases} \\ \overset{B_2(\lambda)}{\rightarrow} CH + H_2 + H \end{cases} \tag{1}$$

where the $B_i(\lambda)$ and $B_{ii}(\lambda)$ are uncertain wavelength-dependent probabilities such that

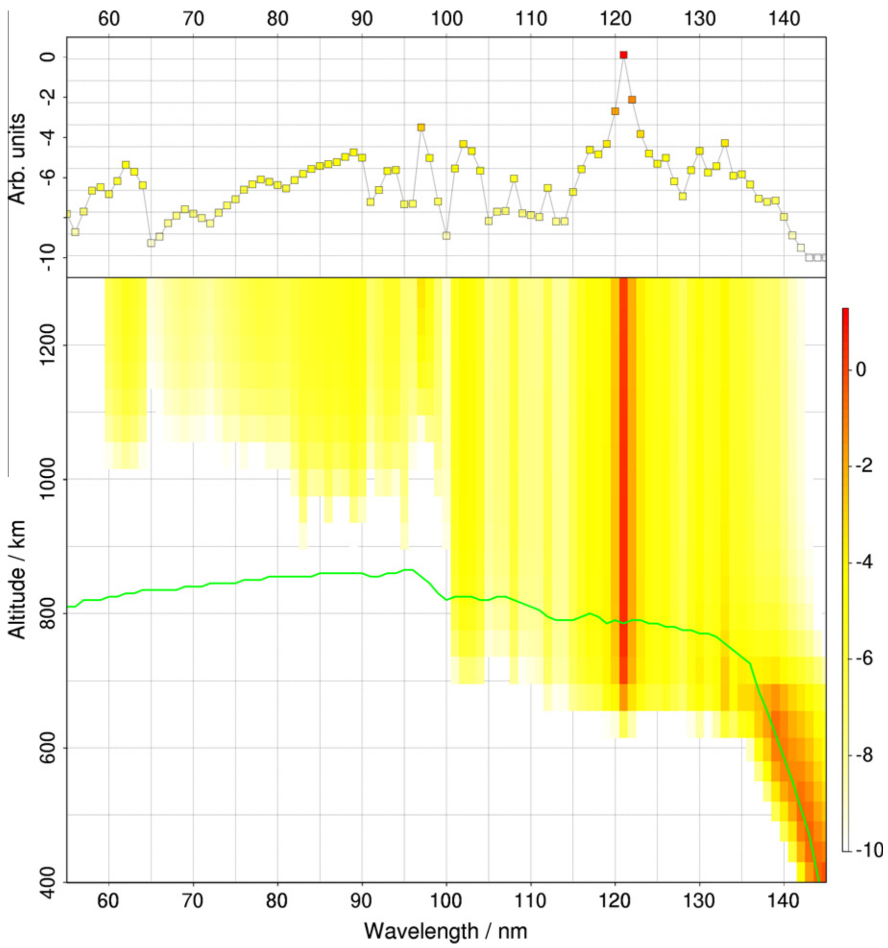

Fig. 4. Weighted photolysis rates $W_\lambda(z) = J_\lambda(z)/\bar{J}(z)$ for CH_4, showing the relative contributions of different wavelength groups to methane destruction. The colors correspond to the values of $-\ln(1/W_\lambda(z) - 1)$, as reported in the color scale. The green line represents the unity optical depth. The upper panel shows the profile of $-\ln(1/W_\lambda(z) - 1)$ at the top of the atmosphere. (For interpretation of the references to color in this figure legend, the reader is referred to the web version of this article.)

$$\begin{aligned}
&B_1(\lambda) * B_{11}(\lambda) = \Phi_\lambda(1)\\
&B_1(\lambda) * B_{12}(\lambda) = \Phi_\lambda(2) + \Phi_\lambda(3)\\
&B_1(\lambda) * B_{13}(\lambda) = \Phi_\lambda(5)\\
&B_2(\lambda) = \Phi_\lambda(6)\\
&B_1(\lambda) + B_2(\lambda) = 1\\
&B_{11}(\lambda) + B_{12}(\lambda) + B_{13}(\lambda) = 1
\end{aligned} \tag{2}$$

Note that Mebel et al. (1997) report that the $^1CH_2 + 2H$ is open below 121.3 nm. This channel was neglected in our wavelength-dependent scheme. Also, for wavelengths below the ionization threshold of methane ($\lambda \simeq 80$ nm), this tree should be nested inside a tree accounting for the branching between ions and neutral products, derived from separate measurements of the total absorption cross section and the ionization cross-section

$$CH_4 + h\nu(\lambda) \rightarrow \begin{cases} \overset{I_1(\lambda)}{\rightarrow} \begin{cases} \overset{B_1(\lambda)}{\rightarrow} \begin{cases} \overset{B_{11}(\lambda)}{\rightarrow} CH_3 + H \\ \overset{B_{12}(\lambda)}{\rightarrow} {}^1CH_2 + H_2 \\ \overset{B_{13}(\lambda)}{\rightarrow} {}^3CH_2 + 2H \end{cases} \\ \overset{B_2(\lambda)}{\rightarrow} CH + H_2 + H \end{cases} \\ \overset{I_2(\lambda)}{\rightarrow} ions \ldots \end{cases} \tag{3}$$

In the present study, we use a neutral photochemistry model and consider as a first approximation that the short wavelength VUV photons are predominantly absorbed by N_2. The following developments are thus based on Scheme (Eq. (1)), mostly valid between 100 and 140 nm. Scheme (Eq. (3)) should be considered for other environments, where CH_4 significantly absorbs short wavelength VUV photons, such as the interstellar medium or synchrotron experiments. Note that this scheme should also be updated to accommodate other possible electronic states of the neutral fragments and/or fragmentation patterns of H_2, possibly accessible at higher energies.

3.1.1. Dirichlet-type probability density functions for uncertain branching ratios

To facilitate the representation of uncertain branching ratios, Carrasco and Pernot (2007) and Plessis et al. (2010) designed a toolbox of *knowledge-adapted* Dirichlet-based distributions.

In the absence of information on the branching ratios, the uniform distribution over the simplex (*Diun*) is used, which implements solely the sum-to-one and positivity constraints. When a set of branching ratios and their uncertainty are available, one can use a generalized Dirichlet distribution (*Dirg*), based on a proposition by Lingwall et al. (2008). For the present study, we observed that *Dirg* was too rigid to correctly represent the experimental calibration datasets of Gans et al. (2011). We therefore introduced another generalized Dirichlet distribution, proposed by Connor and Mosimann (1969) and Wong (1998, 2010), called hereafter *Dirw*, and defined in Appendix A. The parameters of the distribution are estimated by the method of moments, as described in Appendix A. Application of this method to the experimental datasets of branching ratios presented in Section 2.2

leads to the *Dirw* distributions reported in Table 3, at 118.2 nm and 121.6 nm.

3.2. A wavelength-dependent model of branching ratios

We apply here the original representation of uncertain branching ratios developed by Carrasco and Pernot (2007) and extended by Plessis et al. (2010) to complex/heterogeneous sets of branching ratios. This work is further generalized here to deal with wavelength-dependent branching ratios.

As mentioned above, the branching ratios strongly differ at 121.6 nm and 118.2 nm. Unfortunately, with the lack of reliable measurements of a complete set of branching ratios at other wavelengths, we can only extrapolate the evolution of these branching ratios between 100 nm (where N_2 starts to be the major absorbing species) and 140 nm (the absorption threshold of methane).

Previous studies (Zhang et al., 2010; Van Harrevelt, 2006) have shown that a conical intersection between two potential energy surfaces in the molecule could be responsible of dramatic changes in the photodissociation dynamics. In this case, the evolution of the branching ratios could exhibit some local drastic changes in such a way that extrapolation from the available sets of branching ratios at 121.6 nm and 118.2 nm is questionable. On the other hand, Lee and Chiang (1983) have measured the fluorescence yield of CH_2(b) produced by methane photolysis in the wavelength range between 106 nm and 142 nm. This measurement allowed them to deduce the branching ratio of the corresponding channel (Channel (4), Table 1). Their study presents a smooth increase of the branching ratio when the wavelength decreases from 142 nm to 102 nm. Although this channel is negligible when compared to the others (Table 2; Gans et al., 2011), one could assume that a same kind of "smooth variation" can be expected for the other photodissociation channels.

These considerations were used to design an interpolation model of the branching ratios outside of the experimental measurements at 118.2 and 121.6 nm, by incorporating as many other constraints as possible.

3.2.1. Available data/constraints

We present here all the data and constraints which were used in the design of the wavelength-dependent branching ratios model. A summary is provided in Table 3.

- The values and uncertainty for b_{CH} at ~106 and 123.6 nm are obtained from Rebbert and Ausloos (1972/73), which report $b_{CH} = 0.059 \pm 0.005$ at $\lambda = 123.6$ nm and $b_{CH} = 0.23 \pm 0.03$ at $\lambda = 104.8 - 106.7$ nm. These data are used to build the normal distributions reported in Table 3.
- The thermodynamic threshold of the CH pathway is 136.9 nm (Mebel et al., 1997), where we assume that b_{CH} is null. Similarly, the threshold for $^3CH_2$ is 135.6 nm, from which upwards we impose $B_{13} = 0$. In practice, this branching ratio vanishes above 128 nm, and we do not have to use the constraint in the algorithm.
- The distributions for $\{B_{11}, B_{12}, B_{13}\}$ at 121.6 and 118.2 nm have been designed from the experimental data of Gans et al. (2011), by the method of moments as described in Section 3.1.1.
- To account for the absence of knowledge for $\{B_{11}, B_{12}, B_{13}\}$, we impose random constraints at the limits of the wavelength grid of interest through uniform Dirichlet distributions (*Diun*):
  – for $^1CH_2$ and CH_3 at 140 nm (below the thermodynamic threshold of $^3CH_2$): $\{B_{11}, B_{12}\} \sim Diun(2)$;
  – for $^1CH_2$, $^3CH_2$ and CH_3 at 100 nm: $\{B_{11}, B_{12}, B_{13}\} \sim Diun(3)$.

Table 3
Constraints on the wavelength-dependent probabilistic tree model of CH_4 photolysis branching ratios. *Diun*(k) is the uniform Dirichlet distribution over the k-simplex; *Dirw*(α_1, α_2; β_1, β_2) is the generalized Dirichlet distribution for three branching ratios (see Appendix A) and $N(\mu, \sigma)$ is the normal distribution with mean μ and standard deviation σ.

λ/nm	Constraints on the branching ratios	Origin
100.0	$\{B_{11}, B_{12}, B_{13}\} \sim Diun(3)$	No data
106.0	$B_2 \sim N(0.23, 0.03)$	Exp. data
118.2	$\{B_{11}, B_{12}, B_{13}\} \sim Dirw(48.80, 7.76;\ 118.76, 19.21)$	Exp. data
121.6	$\{B_{11}, B_{12}, B_{13}\} \sim Dirw(66.26, 13.05;\ 84.39, 1.89)$	Exp. data
123.6	$B_2 \sim N(0.059, 0.005)$	Exp. data
135.6	$B_{13} = 0$	Thermo. threshold
136.9	$B_2 = 0$	Thermo. threshold
140.0	$\{B_{11}, B_{12}\} \sim Diun(2)$	No data

3.2.2. The interpolation model

In order to get a smooth model respecting all the above constraints, we chose to use polynomial functions, designed in order to respect the structure/independence of the data sets. For the probabilistic tree (Eq. (1)), the branching ratios at the two levels, $\{B_i\}$ and $\{B_{1i}\}$ are treated separately and finally combined using Eq. (2). For each level, one performs a five-stages process:

1. generate random sets of data by sampling the stochastic constraints in Table 3;
2. transform these to *logratios* (see Appendix B);
3. perform a polynomial interpolation (degree depending on number of data);
4. generate the values of the polynomial regression on the target wavelength grid;
5. back-transform the results from logratios to branching ratios.

To enforce the geometrical constrains on branching ratios at all wavelengths, we transform the data to the space of logratios (Aitchison, 1986), perform the interpolation in this space and transform the results back to the branching ratios space. The full algorithm is detailed in Appendix B.

This model assumes that the representative samples of the experimental data are uncorrelated. A set of curves generated from this model is displayed in Fig. 5. One can see that the specified constraints (experimental data, thresholds and boundary conditions) are properly accounted for by our construction method. Although it is not visible in this representation, for each element of the sample, the branching ratio curves form quadruplets with unit sum at all wavelengths.

3.2.3. Implementation

The wavelength-dependent model presented above encompasses the large uncertainty on branching ratios in most wavelength regions. It is inherently stochastic and has to be treated accordingly. In this study, we used a Monte Carlo procedure to implement the branching ratios model, in which we generate a representative sample of the $b_i(\lambda)$ curves (Fig. 5) and perform one run of the photochemical model for each element of this sample. The density profiles of all species (the outputs of the photochemical model) for each run are stored and used for statistical analysis. The whole procedure is similar to the one used for uncertainty propagation and sensitivity analysis by Carrasco and Pernot (2007), Carrasco et al. (2008), Plessis et al. (2010, 2012) to deal with non-wavelength-dependent branching ratios, or by other authors to deal with uncertain rate constants in atmospheric chemistry (Dobrijevic and Parisot, 1998; Thompson and Stewart, 1991; Dobrijevic et al., 2003, 2008, 2010; Hébrard et al., 2006, 2007, 2009; Carrasco et al., 2007; Peng et al., 2010, 2012).

Our purpose being to observe the effects of the representation of branching ratios for non-Ly-α wavelengths, all the other uncertain parameters of the model were fixed at their nominal value. This *partial* uncertainty propagation ignores possible interactions between branching ratios and uncertain reaction rates. The impact of this restriction will be discussed below.

3.3. 1D IPSL photochemical model

The IPSL05 1-dimensional model has been first developed by Toublanc et al. (1995). It was built to go from the surface up to 1300 km altitude. It computes photochemical sources and sinks for hydrocarbons and nitriles. It includes molecular diffusion in N_2, as well as eddy diffusion. CH_4 and N_2 abundances are fixed at the surface, while for all other compounds, no surface exchanges are allowed. Condensation is taken into account. At the upper boundary, Jean's escape is computed for atomic and molecular hydrogen (see also the specific study on hydrogen budget: (Lebonnois et al., 2003)). A flux of nitrogen atoms is also included, to take into account the dissociation of N_2 occurring above the upper limit of the model. An additional flux of atomic nitrogen may also be taken into account due to dissociation of N_2 by galactic cosmic rays, following the dissociation profile used by Lara et al. (1996). Photochemistry of benzene was also added after a specific study, including comparison with Jupiter's photochemistry (Lebonnois, 2005).

The present photochemical dataset is based on the work of Hébrard et al. (2006). It contains 543 reactions involving 56 chemical species (hydrocarbons and N-bearing species). The code has been modified for the present study in order to deal with wavelength-dependent branching ratios for methane and to implement the Monte Carlo procedure.

4. Application to the photochemistry of Titan

A sample of 60 random values of the branching ratios was generated from the above described model and used to run the photochemistry code, which represents 1 day of computer time per model on a tabletop computer. This sample size was deemed sufficient to display the effects of interest in this study.

Table 4
Mean mixing ratio $\bar{y}$ and uncertainty factor F_y of selected species for the three scenarii. All values are estimated at 960 km, where CH_3 has its maximal uncertainty factor in Scenario 2.

Species	Scenario 1		Scenario 2		Scenario 3	
	$\bar{y}$	F_y	$\bar{y}$	F_y	$\bar{y}$	F_y
H	5.45e−04	1.03	5.04e−04	1.07	4.50e−04	1.09
$^3CH_2$	1.11e−07	1.04	1.27e−07	1.11	1.47e−07	1.15
CH_3	2.50e−05	1.09	1.18e−05	1.28	1.20e−05	1.37
C_2H_2	2.24e−04	1.00	2.30e−04	1.01	2.30e−04	1.01
C_2H_4	3.21e−04	1.01	3.37e−04	1.02	3.40e−04	1.02
C_2H_6	2.22e−05	1.02	1.90e−05	1.04	1.96e−05	1.05
C_3H_4	3.22e−05	1.01	3.36e−05	1.02	3.39e−05	1.02
C_3H_8	3.88e−08	1.02	3.31e−08	1.03	3.50e−08	1.04
C_4H_8	1.41e−08	1.00	1.39e−08	1.03	1.49e−08	1.03
C_4H_{10}	2.45e−09	1.01	2.62e−09	1.03	2.65e−09	1.04
C_6H_6	5.57e−07	1.02	6.22e−07	1.06	6.59e−07	1.08
HCN	2.65e−04	1.01	2.51e−04	1.02	2.50e−04	1.03
C_2N_2	1.05e−06	1.05	1.52e−06	1.11	1.50e−06	1.14
HC_2N_2	3.57e−14	1.06	5.35e−14	1.14	5.46e−14	1.18
C_2N	8.53e−11	1.07	5.15e−11	1.23	4.77e−11	1.30

4.1. Branching ratios scenarii

Three scenarii were considered in order to estimate the effects of non-Ly-α branching ratios on the predictions of the photochemical model:

- Scenario 1 implements the dichotomous model commonly found in Titan's photochemical models, i.e. the values of the branching ratios at Ly-α are taken from our reference sample, and the values of the branching ratios for the other wavelengths are fixed at

$$\{b_{CH_3}, b_{^3CH_2}, b_{^1CH_2}, b_{CH}\}_{\lambda \neq 121.6} = \{1, 0, 0, 0\};$$

- Scenario 2 uses the full wavelength-dependent branching ratio curves (Fig. 5);
- Scenario 3 is based on Scenario 2, but aggregates the two electronic states of CH_2 and considers only the production of the excited state, i.e. $b_{^1CH_2}(\text{Scenario 3}) = b_{^3CH_2} + b_{^1CH_2}$ (Scenario 2).

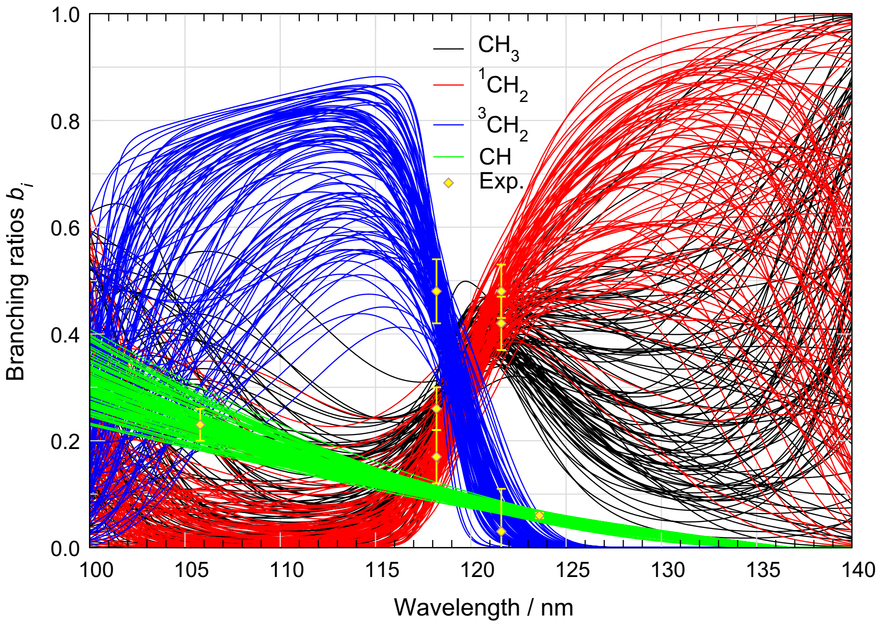

Fig. 5. Sample of simulated wavelength-dependent branching ratios: (black) b_{CH_3}; (red) $b_{^1CH_2}$; (blue) $b_{^3CH_2}$; (green) b_{CH}. The experimental data are represented as yellow bullets with 1σ uncertainty bars. (For interpretation of the references to color in this figure legend, the reader is referred to the web version of this article.)

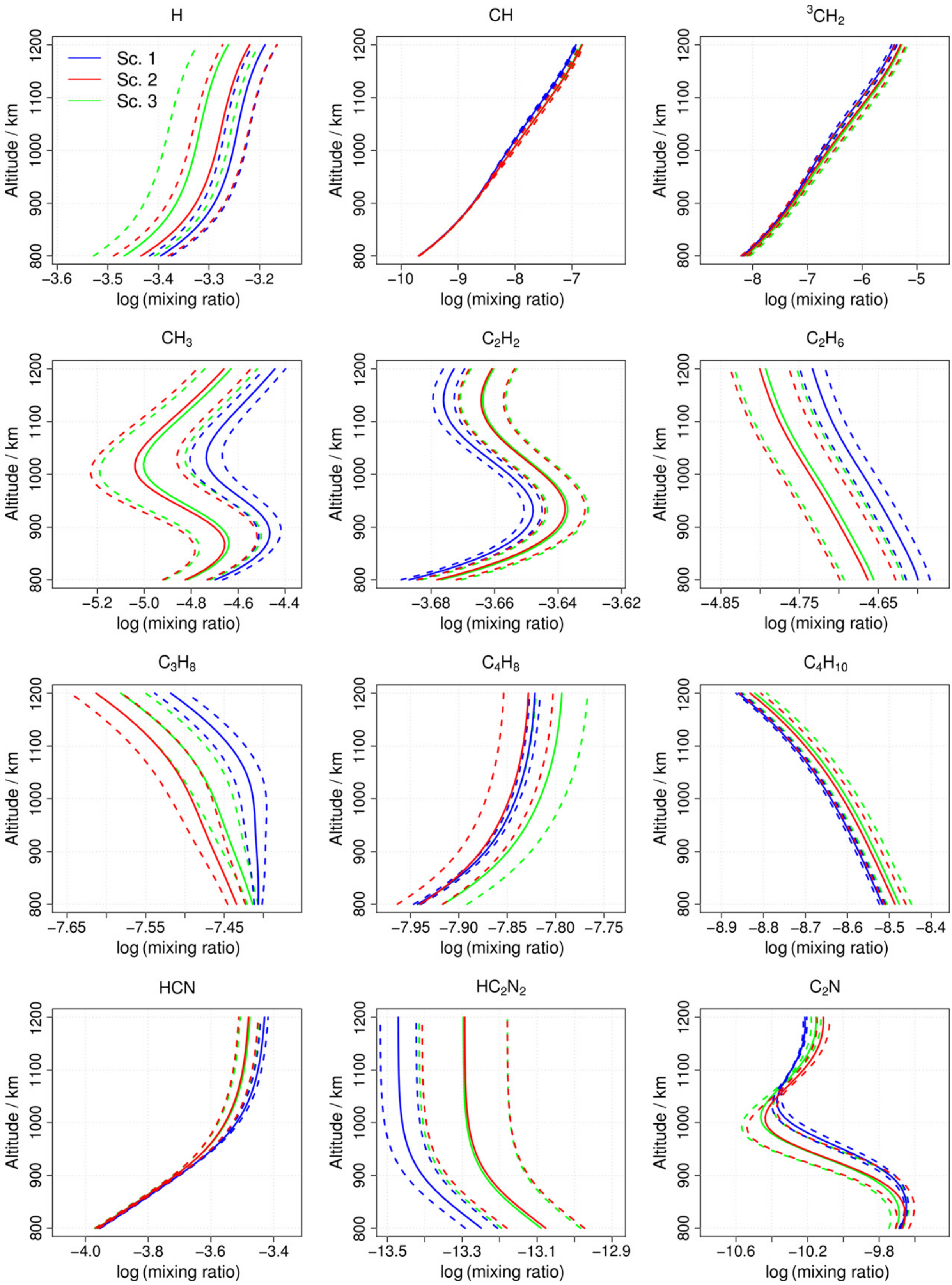

Fig. 6. Mean (full) and 95% confidence intervals (dashes) of altitude-dependent mixing ratios for a set of representative minor species in the upper atmosphere (800–1200 km): (blue) Scenario 1, implementing a fixed value of the branching ratios at non-Ly-α wavelengths ($b_{CH_3} = 1$); (red) Scenario 2, implementing the new wavelength-dependent branching ratios model; (green) Scenario 3, with $b_{^1CH_2}$ (Scenario 3) $= b_{^3CH_2} + b_{^1CH_2}$ (Scenario 2). (For interpretation of the references to color in this figure legend, the reader is referred to the web version of this article.)

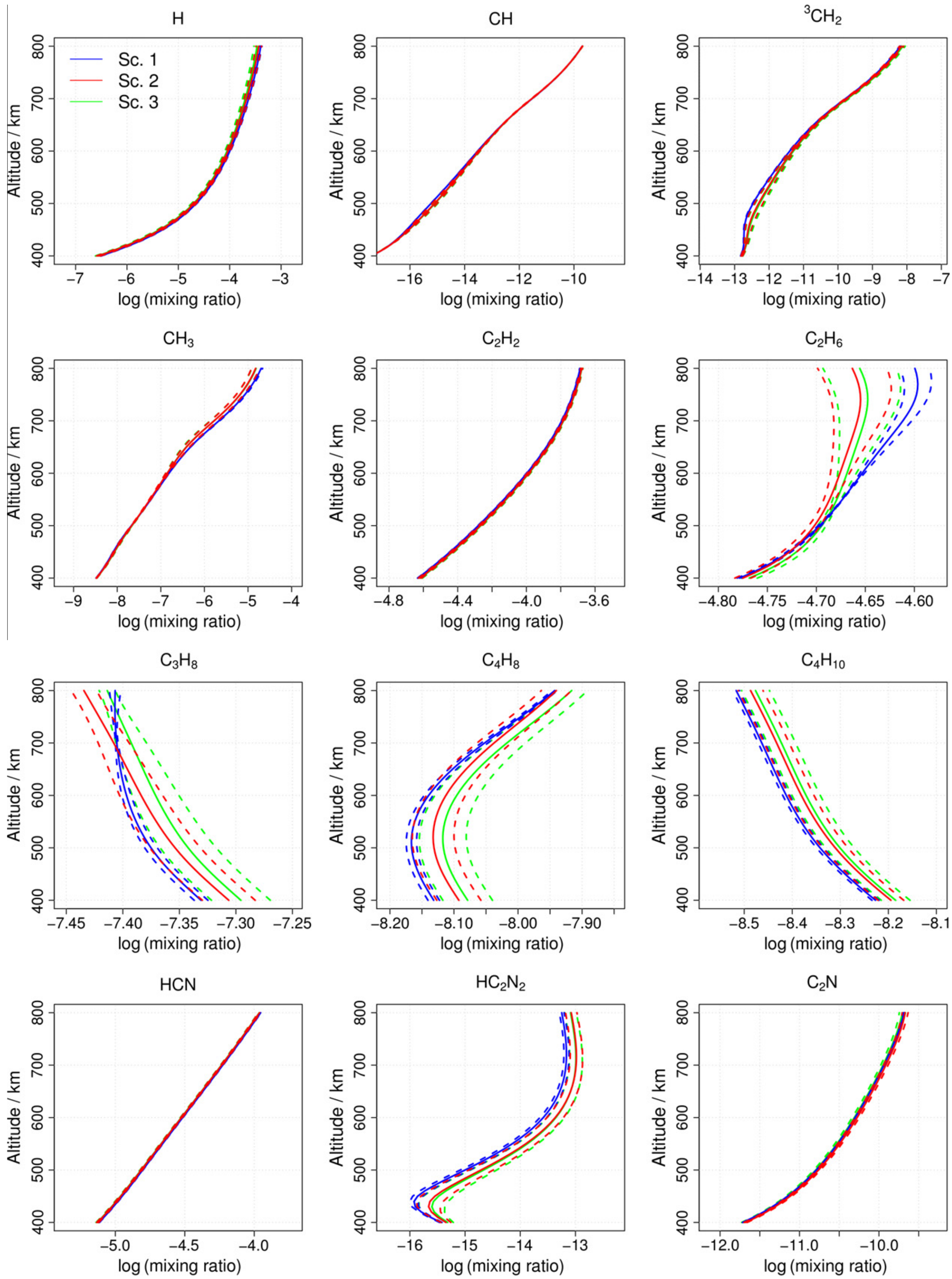

Fig. 7. Same as Fig. 6, with the focus on the 400–800 km range.

The comparison of Scenarii 1 and 2, differing only in the representation of the branching ratios at non-Ly-α wavelengths, should enable to estimate the impact of the non-Ly-α photolysis on the production of minor species and on the corresponding prediction uncertainty. The comparison of Scenarii 2 and 3 is designed to evaluate the importance of discriminating the production pathways of the CH_2 singlet and triplet states in Titan's atmosphere, knowing that the singlet state should be efficiently quenched by N_2 (Wilson and Atreya, 2000).

For each Monte Carlo run, the mixing ratios of all species in the model were stored, and analyzed *a posteriori* to get, for each species, the mean value ($\bar{y}$) and standard uncertainty factor ($F_y = {}^{10}\sigma(\log y)$), where $\sigma(\log y)$ is the standard deviation of the log of the mixing ratio y (Table 4). Note that the relative uncertainty is related to the uncertainty factor by $\sigma(y)/\bar{y} \simeq F_y - 1$.

Figs. 6 and 7 present, for the three scenarii, the mean values and 95% confidence intervals $\left[\bar{y}/F_y^2; \bar{y} \times F_y^2\right]$ for a set of representative species.

If one considers Scenario 1, most species display a very weak sensitivity to the uncertainty in the Ly-α branching ratios. If one estimates the relative uncertainty on the branching ratios to be about 10%, many mixing ratios appear to have a lower relative uncertainty (Table 4). For CH_3, the maximal uncertainty occurs at 960 km with $F \simeq 1.1$, i.e. a 10% relative uncertainty. For all other hydrocarbons, the uncertainty factor remains below 1.04. On the other hand, N-bearing species are more sensitive, although mostly at altitudes where their mixing ratio decays rapidly. For instance, the uncertainty on $N^4(S)$ mixing ratio reaches $F = 1.4$ at 800 km, where the value is more than 100 times smaller than its maximal mixing ratio (not shown). An exception is C_2N which uncertainty reaches $F \simeq 1.1$ around its maximal mixing ratio at 900 km.

When relaxing the strong constraint on non-Ly-α branching ratios (from Scenario 1 to Scenario 2), uncertainty factors get larger for most species, with a notable increase for CH_3 and C_2N. In most cases however, the uncertainty factor remains rather small, on the order of a few percents (Table 4). More notably, the mean values of some species are significantly changed, in the sense that the confidence intervals issued from both scenarii do not overlap: CH_2, CH_3, C_2H_6, C_3H_8, C_4H_8, C_4H_{10}, HCN, HC_2N_2, C_2N, etc.

The results of Scenario 3 differ only slightly from those of Scenario 2, with a notable difference in the mixing ratios of some of the heavier hydrocarbons like C_3H_8, C_4H_8 or C_6H_6, which become more abundant for an increased production of $^1CH_2$ (Fig. 6). A correlation analysis between the inputs and outputs samples points to a pathway implying C_2H_5 and C_3H_7 radicals.

4.2. Discussion

In their local sensitivity study, Wilson and Atreya (2000) tested four deterministic scenarii at Ly-α, based on propositions of Mordaunt et al. (1993) (2 scenarii), Romani (1996) and Smith and Raulin (1999). They observed only minor effects for the smaller hydrocarbons, but major variations for the C_3 species present in their model (C_3H_4 and C_3H_6). In consequence, they retained the nominal scheme of Romani (1996) which provides intermediate results. Note that this scheme is very close at Ly-α to the branching ratios of Gans et al. (2011) implemented in our study, except for the partition between $^1CH_2$ and $^3CH_2$. They complemented their exploration by comparing three schemes out of Ly-α, with a varying balance between CH_3 and $^1CH_2$, from which they observed only minor effects, the largest being a 65% variation in C_2H_6 abundance.

The present study differs from this previous works on a few main points: (i) the chemical model of Hébrard et al. (2006) includes larger hydrocarbons and N-bearing species; (ii) we adopt a probabilistic method in which many schemes are covered by uncertainty modeling; and (iii) we adopt a continuous, wavelength-dependent model of branching ratios accounting for all recent measurements (Scenario 2) and compare it to the commonly used "100% CH_3" out-of-Ly-α scheme (Scenario 1).

We observe for each scenario that the uncertainty in the branching ratios accounted for by our model (about 10%, see Table 1) results in very small prediction uncertainties for most stable hydrocarbons (about 1–4%, see Table 4). Therefore, in agreement with Wilson and Atreya (2000), we observe only weak effects of branching ratios on the smaller hydrocarbons, but also on the heavier ones. By contrast, more notable uncertainties are obtained for N-bearing species, of same order as those of CH_3 or CH_2. This

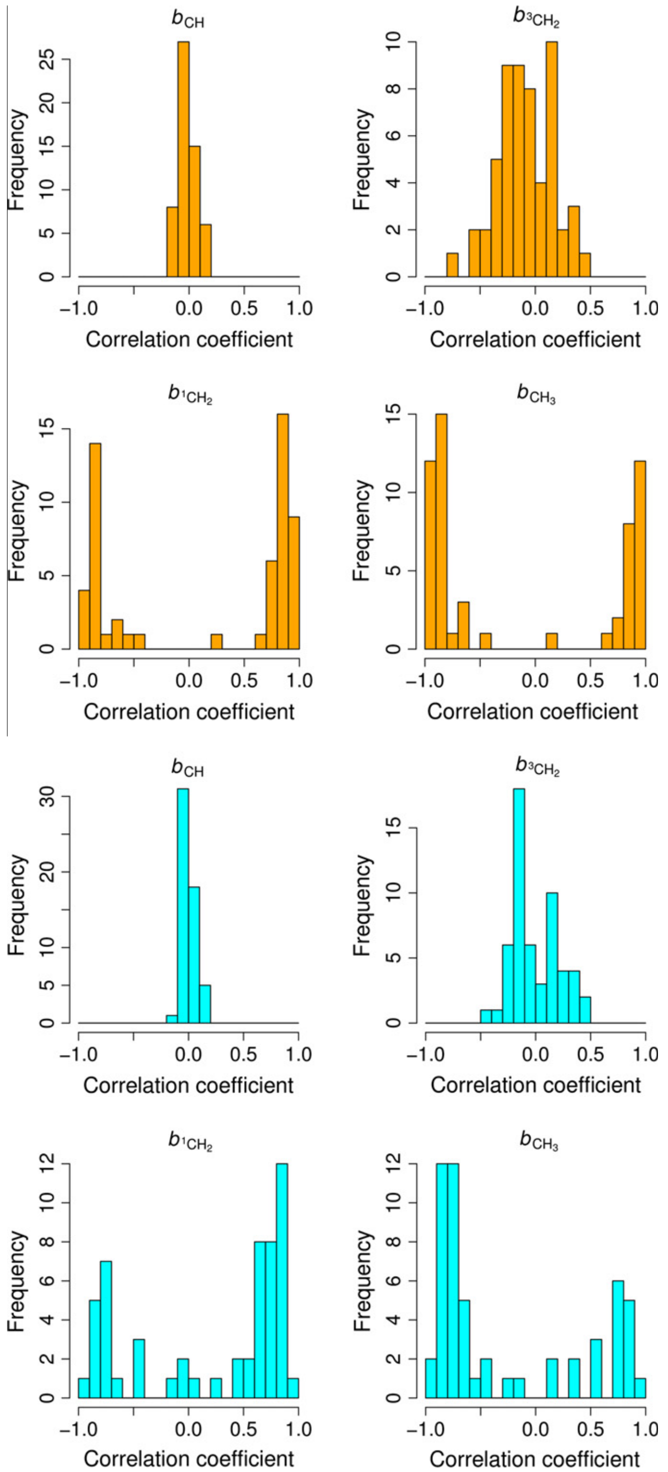

Fig. 8. Sensitivity analysis of the CH_4 branching ratios. (Top/orange) histograms of the linear input/output correlation coefficients, where the inputs are the branching ratios of the Scenario 2 sample at Ly-α, and the outputs are the log mole fractions of all 56 neutral species at 960 km. (Bottom/cyan) same as above, but for a wavelength of 140 nm and mole fractions at 600 km. (For interpretation of the references to color in this figure legend, the reader is referred to the web version of this article.)

sensitivity might be explained by the present sparsity of the chemical scheme for these species. A similar effect was observed for the C_3 species by Wilson and Atreya (2000), as they were terminal species (sinks) in their chemical scheme. The more complete hydrocarbons model of Hébrard et al. (2006) partially annihilates this effect on the C_3 species.

4.2.1. Effect of CH_2 singlet/triplet partition

A notable difference between the branching ratios at Ly-α of Romani (1996) and Gans et al. (2011) is the proportion between the electronic states of CH_2. Considering the small difference between Scenario 2 ($^1CH_2$:$^3CH_2$ = 0.48:0.03) and Scenario 3 (0.51:0.00), the observed variations for some species, such as C_3H_8 or C_4H_8, reveal a marked sensitivity of those species. Nevertheless, this remains a second order effect in comparison with the CH_2:CH_3 partition.

4.2.2. Effect of the CH_2:CH_3 partition

To evaluate the importance of the CH_4 photofragments for the subsequent chemistry, we calculated the linear correlation coefficients between the inputs (branching ratios) and outputs (mole fractions) and summarized them as histograms (Fig. 8). The more influential branching ratios are expected to display larger values of the correlation coefficients, independently of their magnitude (Plessis et al., 2012). This was done for two altitudes: 960 km, and a lower altitude (600 km) where Ly-α has been fully absorbed.

At both altitudes, the branching ratios for $^1CH_2$ and CH_3 have markedly large correlation coefficients with most species (typically above 0.5 in absolute value), which is not the case for the other branching ratios. As stated above, the partition amongst electronic states of CH_2 is secondary. Similarly, considering the histogram of input/outputs correlation coefficients in Fig. 8, b_{CH} does not have a notable influence on any specific species (all correlation coefficients close to 0). This points out the importance of the accuracy of the CH_2:CH_3 partition in the photolysis of CH_4 for the precision of model predictions.

4.2.3. Comparison with the global chemical uncertainty

The previous simulations have shown the impact of various representations of the methane photolysis branching ratios on the mixing ratios of minor species, notably that wavelength-dependent representations of branching ratios out-of-Ly-α (Scenarii 2 and 3) predict mixing ratio profiles that differ significantly from the "100% CH_3" out-of-Ly-α scheme (Scenario 1).

For a better legibility, we had fixed all other chemical parameters to their nominal value. It is important to recast this study in the more global context, where the uncertainty of all chemical parameters is accounted for. To do this we compared the 95% confidence intervals (CIs) obtained in the present study to those predicted by Hébrard et al. (2009). The latter CIs were obtained by applying the altitude-dependent uncertainty factors of Hébrard et al. (2009) to the mean curves of the present study. As shown in Fig. 9, the effect is large enough to justify this approximate CI evaluation: for all species, the inter-scenarii difference is much smaller than the overall uncertainty. Even for CH_3, the present level of accuracy on the branching ratios is sufficient to conclude that other chemical parameters are responsible for its mixing ratio uncertainty in Titan's atmosphere.

There remains the possibility of interactions between uncertain branching ratios and uncertain rate constants. The study of Hébrard et al. (2009) makes use of the Scenario 1 and therefore includes such interactions, albeit restricted to the Ly-α wavelength. Considering the very large prediction uncertainty of the model

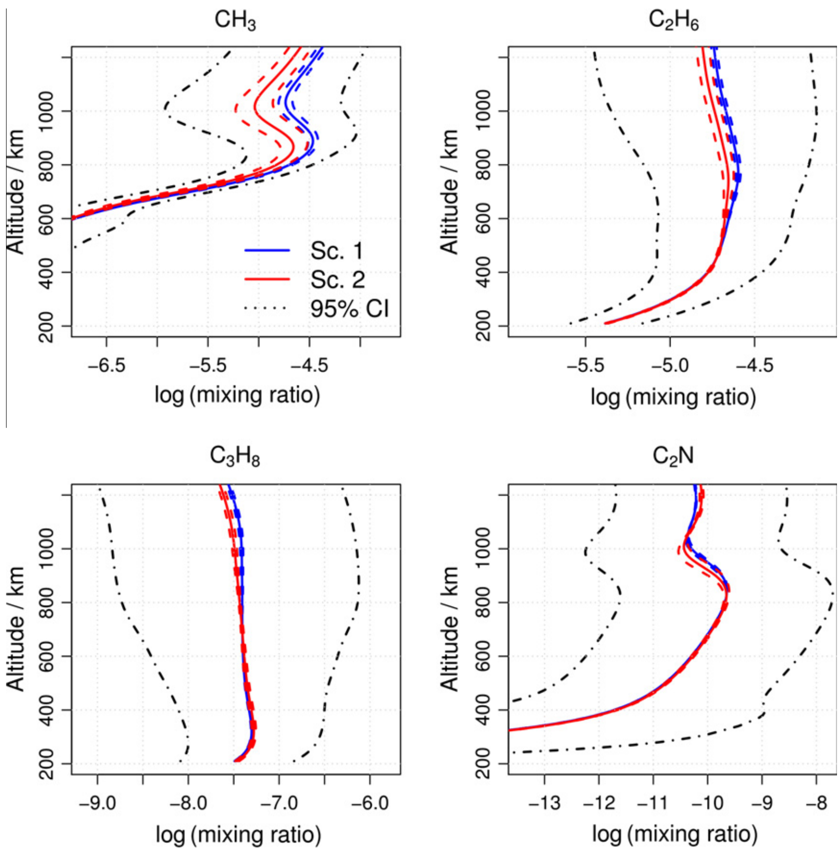

Fig. 9. Same as Fig. 6 for a subset of the species, with (dash-dot) limit profiles of 95% (2σ) confidence interval (CI), obtained when considering all uncertain chemical and photochemical rate constants (Hébrard et al., 2009).

accounting for all chemical uncertainty sources in Titan atmospheric chemistry, it is unlikely that the small contribution of out-of-Ly-α branching ratios evidenced here could contribute significantly to major modifications of the mean mixing ratios, nor to an overall increase of the prediction uncertainty. Nevertheless, this might become a key factor when other uncertainty sources (the key reactions identified by Hébrard et al. (2009)) will have been better constrained.

At this date, we consider that there is very little to be gained in overall precision for Titan models by refining the present CH_4 branching ratios data. One has however to keep in mind that the situation might be completely different in other irradiation conditions, such as in synchrotron-coupled reactors or in the interstellar medium (Fig. 3), where Ly-α is not necessarily so dominant. In this perspective, additional measurements at wavelengths between 121.6 and 140 nm would be most welcomed.

5. Conclusion

In the present study, we built a wavelength-dependent branching ratios description for the photolysis of CH_4 in a photochemical model of Titan. It was shown that the model is mainly sensitive to the CH_2/CH_3 ratio, and that a slight bias is introduced in the models when neglecting the electronic state description of CH_2.

Methane photolysis is mainly driven by Lyman-α wavelength, and the corresponding branching ratios have been updated in detail in the study of Gans et al. (2011). They found values in agreement with the previous experimental based determinations of Romani (1996) and Brownsword et al. (1997), i.e. a rather balanced production of CH_3 and CH_2 radicals. Those ratios were implemented in the Titan's photochemical models of Wilson and Atreya (2004) and in De La Haye et al. (2008) and Bell et al. (2010). On the other hand, several models used the experimental values of Wang et al. (2000) to describe methane photolysis branching ratios at Ly-α: those should be updated, because the production of CH_2 radicals is significantly higher in the determination of Wang and coworkers, which could lead to an overestimation of the CH_2 chemistry chain.

We have also shown some significant contributions of non-Ly-α wavelengths (in particular in the 130–140 nm range) to the methane photolysis budget at altitudes between 400 and 700 km. This highlights a need of accurate *ab initio* calculations and/or extended non-Ly-α branching ratios measurements in the 130–140 nm wavelength range. Moreover, the 500–700 km altitude range corresponds to an unprobed atmospheric layer, either by the Cassini instruments or by remote sensing. Indeed the *in situ* instruments explore Titan's atmosphere down to 900 km, whereas remote sensing instruments probe the atmosphere up to 500 km (Brown et al., 2009). The so-called "nodatasphere" between 500 and 900 km can presently only be studied by photochemical models, except for a single measurement during the descent of the Huygens probe in 2005. This change of photolysis regime around 650 km shows the necessity of models to understand the photochemistry in this region. Without any study yet on the branching ratios at 130–140 nm wavelength range, those have to be extrapolated in the models. Two simple extrapolation patterns were found in the literature: a "100% CH_3" scenario, and a Ly-α-like scenario. These arbitrary scenarii were compared to our wavelength-dependent one. The "100% CH_3" scenario positively bias the major saturated hydrocarbons density profiles (such as ethane C_2H_6 and propane C_3H_8) and should be avoided.

Finally, Ly-α is actually the predominant wavelength driving most of the photochemistry in the Solar System atmospheres, but it is not the case in other systems. The proper wavelength description of methane photolysis branching ratios developed in the present study may also directly be used to interpret methane photochemistry induced in lab simulations with VUV sources necessarily different from the solar spectrum, or for chemical models *of the interstellar medium* (van Dishoeck and Black, 1982).

Acknowledgements

The authors thank A. Giuliani (SOLEIL) for providing the DISCO VUV spectrum. Financial support from the "Pôle Planétologie" of the PRES UniverSud Paris is acknowledged (Contract 2008-53).

Appendix A. The *Dirw* generalized Dirichlet distribution

We present here the definition of this distribution, proposed by Connor and Mosimann (1969) and Wong (1998, 2010), and the method of moments to estimate its parameters from a sample of branching ratios.

A.1. Definition

For a set of $k+1$ variables, the probability density function for the first k variables ($X_1 + X_2 + \cdots + X_k \leqslant 1$) depends on $2k$ parameters ($\alpha_1, \ldots, \alpha_k, \beta_1, \ldots, \beta_k$),

$$f(X_1, \ldots, X_k;\ \alpha_1, \ldots, \alpha_k, \beta_1, \ldots, \beta_k) = \prod_{i=1}^{k} \frac{\Gamma(\alpha_i + \beta_i)}{\Gamma(\alpha_i)\Gamma(\beta_i)} X_i^{\alpha_i - 1}(1 - X_1 - \cdots - X_i)^{\gamma_i} \tag{A.1}$$

where $\gamma_i = \beta_i - \alpha_{i+1} - \beta_{i+1}$ for $i = 1, 2, \ldots, k-1$, and $\gamma_k = \beta_k - 1$.

The following notation is used in the text

$$\{X_1, \ldots, X_{k+1}\} \sim Dirw(\alpha_1, \ldots, \alpha_k; \beta_1, \ldots, \beta_k). \tag{A.2}$$

A.2. The method of moments

The parameters ($\alpha_1, \ldots, \alpha_k, \beta_1, \ldots, \beta_k$) of the *Dirw* distribution can be identified with different methods: bayesian inference (Maximum A Posteriori estimation) (Gregory, 2005) and the method of moments (Wong, 2010). We checked that both methods provide similar results. We present here the faster method of moments.

By transforming the original variables $X_1, \ldots, X_k$ to a new set of variables $Z_1, \ldots, Z_k$ by

$$Z_1 = X_1 \tag{A.3}$$

$$Z_i = X_i/(1 - X_1 - \cdots - X_{i-1}) \tag{A.4}$$

one obtains independent variables with Beta distribution $Z_i \sim Beta(\alpha_i, \beta_i)$ (Evans et al., 2000). The values of the parameters can be directly obtained from samples of the transformed data by inversion of the formulae for the mean and variance

$$E(Z_i) = \frac{\alpha_i}{\alpha_i + \beta_i} \tag{A.5}$$

$$Var(Z_i) = \frac{\alpha_i \beta_i}{(\alpha_i + \beta_i)^2(1 + \alpha_i + \beta_i)} \tag{A.6}$$

i.e.

$$\alpha_i = E(Z_i)^2(1 - E(Z_i))/Var(Z_i) - 1 \tag{A.7}$$

$$\beta_i = E(Z_i)(1 - E(Z_i))^2/Var(Z_i) - 1. \tag{A.8}$$

Appendix B. Generation of wavelength-dependent branching ratios

Preamble. Any composition $\{x_1, \ldots, x_n\}$ with constraint $\sum_{i=1}^{n} x_i = 1$ can be transformed to $\mathbb{R}^n$ by using logratios. For instance, the centered logratio (clr) transform $\{z_1, \ldots, z_n\} = \text{clr}\{x_1, \ldots, x_n\}$ is defined by $z_i = \ln(x_i/c)$, where $c = \left(\Pi_{i=1}^{n} x_i\right)^{1/n}$ is the geometric mean of the composition. The inverse transform (clrinv) is $x_i = \exp(z_i)/\sum_{j=1}^{n} \exp(z_j)$.

We present here the algorithm used to sample from the probabilistic tree model (Eq. (1)).

1. Define the target wavelength grid $\{\lambda_j; j = 1, N_\lambda\}$.
2. To generate a sample of branching ratios curves on this grid, repeat the following sequence:
   (a) Generate a random curve $\{B_2(\lambda_j)\}$
      (i) Generate a triplet of values $\{x^{(1)}, x^{(2)}, x^{(3)}\}$ at the three reference wavelengths {105.8, 123.6, 136.9} by sampling the corresponding distributions in Table 3.
      (ii) Transform these values to logratios $\{z^{(1)}, z^{(2)}, z^{(3)}\}$ by clr.
      (iii) Generate the quadratic interpolation of $\{z^{(1)}, z^{(2)}, z^{(3)}\}$ over the wavelength grid of interest $\{z(\lambda_j)\}$.
      (iv) For each point of the wavelength grid, back transform $\{z(\lambda_j)\}$ to get $B_2(\lambda_j)$.
   (b) Generate random curves for $\{B_{11}(\lambda), B_{12}(\lambda), B_{13}(\lambda)\}$
      (i) Generate a quadruplet of compositions $\left\{\left\{x_1^{(i)}, x_2^{(i)}, x_3^{(i)}\right\}; i = 1, 4\right\}$ at the reference wavelengths {110, 118.2, 121.6, 140}.
      (ii) For each reference wavelength i transform the composition values to logratios $\left\{z_1^{(i)}, z_2^{(i)}, z_3^{(i)}\right\} = \text{clr}\left\{x_1^{(i)}, x_2^{(i)}, x_3^{(i)}\right\}$.
      (iii) For each pathway k, generate the cubic interpolation of $\left\{z_k^{(1)}, z_k^{(2)}, z_k^{(3)}, z_k^{(4)}\right\}$ over the wavelength grid of interest $\{z_k(\lambda_j)\}$.
      (iv) At each point of the target wavelength grid, back transform the logratios
      $$\{B_{11}(\lambda_j), B_{12}(\lambda_j), B_{13}(\lambda_j)\} = \text{clrinv}\{z_1(\lambda_j), z_2(\lambda_j), z_3(\lambda_j)\}$$
   (c) For each point of the wavelength grid, combine the values of both levels of the tree
      $$\begin{aligned} b_{CH_3}(\lambda_j) &= B_{11}(\lambda_j) * (1 - B_2(\lambda_j)) \\ b_{CH_2(a)}(\lambda_j) &= B_{12}(\lambda_j) * (1 - B_2(\lambda_j)) \\ b_{CH_2(X)}(\lambda_j) &= B_{13}(\lambda_j) * (1 - B_2(\lambda_j)) \\ b_{CH}(\lambda_j) &= B_2(\lambda_j). \end{aligned}$$

References

Aitchison, J., 1986. The Statistical Analysis of Compositional Data. Monographs on Statistics and Applied Probability. Chapman and Hall, London.

Atreya, S.K., 2007. Titan's organic factory. Science 316, 843–845.

Bell, J.M. et al., 2010. Simulating the one-dimensional structure of Titan's upper atmosphere: 1. Formulation of the Titan Global Ionosphere–Thermosphere Model and benchmark simulations. J. Geophys. Res. 115, E12002.

Brown, R., Lebreton, J.-P., Waite, H., 2009. Titan from Cassini–Huygens. Springer, doi:10.1007/978-1-4020-9215-2.

Brownsword, R.A., Hillenkamp, M., Laurent, T., Vatsa, R.K., Volpp, H.R., Wolfrum, J., 1997. Quantum yield for H atom formation in the methane dissociation after photoexcitation at the Lyman-α (121.6 nm) wavelength. Chem. Phys. Lett. 266, 259–266.

Carrasco, N., Pernot, P., 2007. Modeling of branching ratio uncertainty in chemical networks by Dirichlet distributions. J. Phys. Chem. A 111, 3507–3512.

Carrasco, N., Hébrard, E., Banaszkiewicz, M., Dobrijevic, M., Pernot, P., 2007. Influence of neutral transport on ion chemistry uncertainties in Titan ionosphere. Icarus 192, 519–526.

Carrasco, N. et al., 2008. Sensitivity of a Titan ionospheric model to the ion-molecule reaction parameters. Planet. Space Sci. 55, 1644–1657.

Connor, R.J., Mosimann, J.E., 1969. Concepts of Independence for proportions with a generalization of the Dirichlet distribution. J. Am. Stat. Assoc. 64, 194–206.

Cook, P.A., Ashfold, M.N.R., Jee, Y.J., Jung, K.H., Harich, S., Yang, X.M., 2001. Vacuum ultraviolet photochemistry of methane, silane and germane. Phys. Chem. Chem. Phys. 3, 1848–1860.

De La Haye, V., Waite, J., Cravens, T., Robertson, I., Lebonnois, S., 2008. Coupled ion and neutral rotating model of Titan's upper atmosphere. Icarus 197, 110–136.

Dobrijevic, M., Parisot, J.P., 1998. Effect of chemical kinetics uncertainties on hydrocarbon production in the stratosphere of Neptune. Planet. Space Sci. 46, 491–505.

Dobrijevic, M., Ollivier, J., Billebaud, F., Brillet, J., Parisot, J., 2003. Effect of chemical kinetic uncertainties on photochemical modeling results: Application to Saturn's atmosphere. Astron. Astrophys. 398, 335–344.

Dobrijevic, M., Claeys-Bruno, M., Sergent, M., Phan-Tan-Luu, R., 2008. Experimental designs for the determination of key reactions in photochemical models: Application to the photochemistry of hydrocarbons in the atmosphere of Titan. Planet. Space Sci. 56, 519–529.

Dobrijevic, M., Hébrard, E., Plessis, S., Carrasco, N., Bruno-Claeys, M., Pernot, P., 2010. Comparison of methods for the determination of key reactions in chemical systems: Application to Titan's atmosphere. Adv. Space Res. 45, 77–91.

Evans, M., Hastings, N., Peacock, B., 2000. Statistical Distributions, third ed. Wiley-Interscience.

Gans, B. et al., 2010. Determination of the absolute photoionization cross sections of CH_3 and I produced from a pyrolysis source, by combined synchrotron and vacuum ultraviolet laser studies. J. Phys. Chem. A 114, 3237–3246.

Gans, B. et al., 2011. Photolysis of methane revisited at 121.6 nm and at 118.2 nm: Quantum yields of the primary products, measured by mass spectrometry. Phys. Chem. Chem. Phys. 13, 8140–8152.

Giuliani, A. et al., 2009. DISCO: A low-energy multipurpose beamline at synchrotron SOLEIL. J. Synchrotron Radiat. 16, 835–841.

Gregory, P.C., 2005. Bayesian Logical Data Analysis for the Physical Sciences. Cambridge University Press, Cambridge, UK.

Hébrard, E., Dobrijevic, M., Bénilan, Y., Raulin, F., 2006. Photochemical kinetics uncertainties in modeling Titan's atmosphere: A review. J. Photochem. Photobiol. A: Chem. 7, 211–230.

Hébrard, E., Dobrijevic, M., Bénilan, Y., Raulin, F., 2007. Photochemical kinetics uncertainties in modeling Titan's atmosphere: First consequences. Planet. Space Sci. 55, 1470–1489.

Hébrard, E. et al., 2009. How measurements of rate coefficients at low temperature increase the predictivity of photochemical models of Titan's atmosphere. J. Phys. Chem. A 113, 11227–11237.

Krasnopolsky, V., 2009. A photochemical model of Titan's atmosphere and ionosphere. Icarus 201, 226–256.

Lara, L., Lellouch, E., Lopez-Moreno, J., Rodrigo, R., 1996. Vertical distribution of Titan's atmospheric neutral constituents. J. Geophys. Res. 101, 261–283.

Lavvas, P., Coustenis, A., Vardavas, I., 2008. Coupling photochemistry with haze formation in Titan's atmosphere, Part I: Model description. Planet. Space Sci. 56, 27–66.

Lavvas, P. et al., 2011. Energy deposition and primary chemical products in Titan's upper atmosphere. Icarus 213, 233–251.

Lebonnois, S., 2005. Benzene and aerosol production in Titan and Jupiter's atmospheres: A sensitivity study. Planet. Space Sci. 53, 486–497.

Lebonnois, S., Toublanc, D., Hourdin, F., Rannou, P., 2001. Seasonal variations of Titan's atmospheric composition. Icarus 152, 384–406.

Lebonnois, S., Bakes, E., McKay, C., 2003. Atomic and molecular hydrogen budget in Titan's atmosphere. Icarus 161, 474–485.

Lee, L.C., Chiang, C.C., 1983. Fluorescence yield from photo-dissociation of CH_4 at 1060–1420 Å. J. Chem. Phys. 78, 688–691.

Lingwall, J., Christensen, W., Reese, C., 2008. Dirichlet based bayesian multivariate receptor modeling. Environmetrics 19, 618–629.

Lodriguito, M.D., Lendvay, G., Schatz, G.C., 2009. Trajectory surface-hopping study of methane photodissociation dynamics. J. Chem. Phys. 131, 224320-1–224320-9.

Mebel, A.M., Lin, S.H., Chang, C.H., 1997. Theoretical study of vibronic spectra and photodissociation pathways of methane. J. Chem. Phys. 106, 2612–2620.

Mordaunt, D.H. et al., 1993. Primary product channels in the photodissociation of methane at 121.6 nm. J. Chem. Phys. 98, 2054–2065.

Park, J., Lee, J., Sim, K., Han, J.W., Yi, W., 2008. Photodissociation of methane at Lyman-α (121.6 nm). Bull. Korean Chem. Soc. 29, 177–180.

Peng, Z., Dobrijevic, M., Hébrard, E., Carrasco, N., Pernot, P., 2010. Photochemical modeling of Titan atmosphere at the 10% uncertainty horizon. Faraday Discuss. 147, 137–153.

Peng, Z., Cailliez, F., Dobrijevic, M., Pernot, P., 2012. Null variance altitudes for the photolysis rate constants of species with barometric distribution: Illustration on Titan upper atmosphere modeling. Icarus 218, 950–955.

Pernot, P., Plessis, S., Carrasco, N., 2011. Probabilistic representations of partial branching ratios: Bridging the gap between experiments and chemical models. J. Phys.: Conf. Ser. 300, 012027-1–012027-8.

Plessis, S., Carrasco, N., Pernot, P., 2010. Knowledge-based probabilistic representations of branching ratios in chemical networks: The case of dissociative recombinations. J. Chem. Phys. 133, 134110-1–134110-21.

Plessis, S., Carrasco, N., Dobrijevic, M., Pernot, P., 2012. Production of neutral species in Titan's ionosphere through dissociative recombination of ions. Icarus 219, 254–266.

Rebbert, R.E., Ausloos, P., 1972/73. Photolysis of methane: Quantum yield of C(^{1}D) and CH. J. Photochem. 1, 171–176.

Romani, P.N., 1996. Recent rate constant and product measurements of the reactions $C_2H_3 + H_2$ and $C_2H_3 + H$ importance for photochemical modeling of hydrocarbons on Jupiter. Icarus 122, 233–241.

Smith, N.S., Raulin, F., 1999. Modeling of methane photolysis in the reducing atmospheres of the outer Solar System. J. Geophys. Res. 104, 1873–1876.

Thompson, A., Stewart, R., 1991. Effect of chemical kinetics uncertainties on calculated constituents in a tropospheric photochemical model. J. Geophys. Res. 96, 13089–13108.
Toublanc, D., Parisot, J.P., Brillet, J., Gautier, D., Raulin, F., McKay, C.P., 1995. Photochemical modeling of Titan's atmosphere. Icarus 113, 2–26.
van Dishoeck, E., Black, J., 1982. The excitation of interstellar C_2. Astrophys. J. 258, 533–547.
Van Harrevelt, R., 2006. Photodissociation of methane: Exploring potential energy surfaces. J. Chem. Phys. 125, 124302-1–124302-8.
Van Harrevelt, R., 2007. First ultraviolet absorption band of methane: An ab initio study. J. Chem. Phys. 126, 204313-1–204313-8.
Waite, J. et al., 2007. The process of tholin formation in Titan's upper atmosphere. Science 316, 870–875.
Wang, J.H., Liu, K., 1998. VUV photochemistry of CH_4 and isotopomers. I. Dynamics and dissociation pathway of the H/D-atom elimination channel. J. Chem. Phys. 109, 7105–7112.
Wang, J.H. et al., 2000. Vacuum ultraviolet photochemistry of CH_4 and isotopomers. II. Product channel fields and absorption spectra. J. Chem. Phys. 113, 4146–4152.
Wilson, E.H., Atreya, S.K., 2000. Sensitivity studies of methane photolysis and its impact on hydrocarbon chemistry in the atmosphere of Titan. J. Geophys. Res. 105, 20263–20273.
Wilson, E.H., Atreya, S.K., 2004. Current state of modeling the photochemistry of Titan's mutually dependent atmosphere and ionosphere. J. Geophys. Res. 109, E06002.
Wilson, E.H., Atreya, S.K., 2009. Titan's carbon budget and the case of the missing ethane. J. Phys. Chem. A 113, 11221–11226.
Wong, T.-T., 1998. Generalized Dirichlet distribution in Bayesian analysis. Appl. Math. Comput. 97, 165–181.
Wong, T.-T., 2010. Parameter estimation for generalized Dirichlet distributions from the sample estimates of the first and the second moments of random variables. Comput. Stat. Data Anal. 54, 1756–1765.
Zhang, Y., Yuan, K., Yu, S., Yang, X., 2010. Highly rotationally excited CH_3 from methane photodissociation through conical intersection pathways. J. Phys. Chem. Lett. 1, 475–479.